Correlations in electrically coupled chaotic lasers

E. J. Rosero,[1] W. A. S. Barbosa,[1] J. F. Martinez Avila,[1,2] A. Z. Khoury,[1,3] and J. R. Rios Leite[1]
[1]*Departamento de Física, Universidade Federal de Pernambuco, 50670-901 Cidade Universitária, Recife, PE, Brazil*
[2]*Departamento de Física, Universidade Federal de Sergipe, Av. Marechal Rondon, S/N Jardim Rosa Elze, 49100-000 São Cristóvão, SE, Brazil*
[3]*Instituto de Física, Universidade Federal Fluminense, Av. Gal. Milton Tavares de Souza S/N, 24210-346 Niteroi, RJ, Brazil*
(Received 1 December 2014; revised manuscript received 17 July 2016; published 12 September 2016)

We show how two electrically coupled semiconductor lasers having optical feedback can present simultaneous antiphase correlated fast power fluctuations, and strong in-phase synchronized spikes of chaotic power drops. This quite counterintuitive phenomenon is demonstrated experimentally and confirmed by numerical solutions of a deterministic dynamical system of rate equations. The occurrence of negative and positive cross correlation between parts of a complex system according to time scales, as proved in our simple arrangement, is relevant for the understanding and characterization of collective properties in complex networks.

DOI: 10.1103/PhysRevE.94.032210

I. INTRODUCTION

For a long time, light-emitting diodes are known to show photon emission correlations depending on their electrical pumping coupling. When parallel connected and pumped by a very regular current source their output has a negative cross correlation [1]. For pairs of diode lasers this quantum optics effect extends into classical antiphase fluctuations in the power emitted by the two lasers [2]. To explain these effects physically one needs to remember that the pump electrical carriers flow and recombine either way between the parallel connected units. Quantum correlations in power fluctuation among pairs of lasers with a common pump source have also been studied many years ago [3] and one can also obtain an intuitive explanation for their behavior. The realm of classical nonlinear dynamics does not always give such simple intuitive results. This will be experimentally shown here for coupled pairs of chaotic diode lasers. The power fluctuations in the lasers present the coexistence of antiphase fluctuations at a fast time scale simultaneously with in-phase, fully chaotic synchronized power drops in a time scale two orders of magnitude slower. The occurrence of anticorrelations in subsystems of complex systems that have collective synchronized states is an intriguing effect pertaining to different domains in nature. One finds it described in economics [4] where the data from antiphase correlated pairs of stocks are proposed to extract the best conditions for investors to make gains. Analogous to what we show for lasers, the antiphase oscillations of stock values may occur as the market changes and even through the events of crashes, when both stocks have a simultaneous huge drop.

In this work we show the dynamics of one pair of lasers chaotic by optical feedback and coupled electrically. The results show how competitive coupling for pump energy among two chaotic subsystems can lead to synchronized pulse spikes in the whole system while antiphase oscillations remain present among the parts. We can optically and electrically probe the variables and this allows detailed experimental inspection of the dynamics and its comparison with the theoretical model. A data series acquired from each subsystem unit can be statistically matched to numerically calculated data, extracted from an autonomous deterministic dynamical system with time delay. The physical interpretation of the equations is available and numerical solutions provide excellent agreement with the experiment. Such mechanisms can have a relevant impact on understanding large laser network dynamics.

From a practical point of view, diode lasers are the most used in optical engineering. The nonlinear behavior of a single edge emitting diode laser with external cavity optical feedback has many dynamical forms as its pump current is changed [5]. Among these are the so-called low frequency fluctuation (LFF) in power. The laser acquires a chaotic regime of fast power fluctuations along with strong power drops with irregular large time intervals. Most of this dynamics can be predicted by a deterministic semiclassical model of rate equations with delay [6,7] and its experimental study is still attracting broad interest in deterministic coherence resonance [8] and optical rogue events created by feedback with conjugated fields [9]. A comprehensive review of laser diode chaos can be found in [10]. Modeled as excitable systems [11–14], they also have been applied to simulate complex networks [15,16].

To have a single diode laser presenting chaotic LFF [5,6,17], an external mirror placed a few meters apart and aligned as an external cavity, feeds back part of the field with a time delay, τ, in the range of tens of nanoseconds. Then, apart from the optical field period close to 10^{-14} s, three time scales can be identified in the intensity instabilities [7,17]:

(1) First there are ultrafast field fluctuations in the 10 ps range. These field amplitude and phase fluctuations result from the *quasimode locking* process among the external cavity modes that creates ultrashort pulses.

(2) Next, the laser output power may show fluctuating modulations in the intermediate feedback time scale on the order of 10 ns, again due to the external reflecting feedback cavity.

(3) Finally, the irregular LFF power drops occur with an average time interval in the 1 μs–1 ms range, another two or more orders of magnitude slower. These instabilities are reproduced theoretically with a deterministic set of equations in a dissipative nonlinear system [7]. All these effects are within classical fluctuations scales. Light and pump currents quantum fluctuations in the experiments are not addressed and consistently the equations are fully deterministic without quantum fluctuation terms.

Optically coupled pairs of the above described lasers have been studied as they present cross-correlated dynamics including chaotic synchronization [18,19], which has fundamental and applied interests [15,20]. Novel dynamical behavior appears and is reported here when, instead of optically coupled, the pair of lasers has optical feedback but is electronically coupled in parallel. Examined with broadband time resolution, the dynamics of each laser has instabilities in the three above referred to time scales. The main new result of our work is the demonstration that the two-laser system does not show the same type of correlations in the different time scales. Synchronism with in-phase correlation at the slow scale is observed along with antiphase power fluctuations at the intermediate faster scale, while no correlation appears in the ultrafast time scale (10 ps range). We also show how simple laser rate equations, including electric current conservation, match the experiments and open the possibility for new numerical studies in laser networks.

II. EXPERIMENTAL SETUP

Let us first describe the experimental setup. Pairs of semiconductor lasers differing by less than 2% in their threshold current and optical frequency were coupled electrically in parallel configuration and pumped by a high impedance current source, as indicated in Fig. 1. Various types of commercial GaAlAs single transverse mode Fabry-Perot lasers were used: one pair of Hitachi-HL8334MG, emitting at 83 nm with a threshold current of 33 mA, a pair of Thorlabs L850P010 with a 10.5 mA threshold current and 850 nm wavelength, and another pair of L780P010 with a threshold of 8.5 mA near 780 nm wavelength. All present the same phenomena. Solitary longitudinal mode separation was typically 150 GHz and no control was used to keep the lasers monomode. The electric coupling between the lasers was made by short coaxial cable connections. The total current was stabilized to ± 0.001 mA and each laser temperature to 0.01 K. Optical feedback was implemented by reflecting dielectric mirrors located at distances between 3.00 and 8.00 m from each laser, after beam collimation by aspheric antireflection coated lenses. Manipulating the optical alignment, up to 6% current threshold reduction could be achieved in both lasers. The feedback delay times were $\tau_j = 40$ ns with a ± 5 ps precision

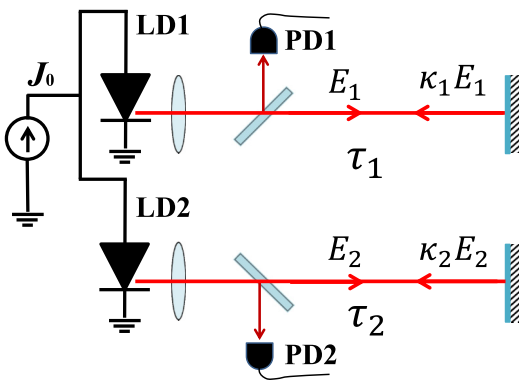

FIG. 1. Setup for the experiments on the power correlations and chaos synchronization of two electrically coupled lasers.

mismatch that did not affect the results. Output coupling beam splitters lead 4% of light onto 3 GHz bandwidth photodiodes. Setting the total pump current near twice the single laser free running threshold, makes each laser present LFF. Output power data series were acquired by a 1 GHz bandwidth digital oscilloscope. The time series were computer treated to calculate experimental histograms and correlation functions. In Sec. V more is given on the experimental electronic details and measurements made in the system.

III. DYNAMICAL EQUATIONS WITH PUMP COUPLING

The theoretical framework to explain the experiments has the simple form of a rate equations dynamical system with time delay. Our model is a pair of coupled equations corresponding to monomode laser equations, having delayed optical field feedback, as introduced by Lang and Kobayashi [6], and Sano [7], supplemented by Kirchhoff's laws, with the constraint imposing constant total electronic pump current, J_0.

$$\frac{dE_j}{dt} = \frac{(1+i\alpha_j)}{2}\left[G_j(N_j) - \frac{1}{\tau_{pj}}\right]E_j(t) + \kappa_j E_j(t-\tau_j), \tag{1}$$

$$\frac{dN_j}{dt} = J_j(t) - \frac{N_j(t)}{\tau_{sj}} - G_j(N_j)|E_j(t)|^2, \tag{2}$$

where the gain for each laser ($j = 1,2$) is given by

$$G_j(N_j) = \frac{G_{0j}[N_j(t) - N_{0j}]}{1 + \epsilon_j |E_j(t)|^2}. \tag{3}$$

In these equations the dynamical variables are the complex optical electric field, $E_j(t)$, and the carrier population inversion, $N_j(t)$. The parameters are the diode laser linewidth enhancement factor α_j, the photon lifetime in the laser chip cavity τ_{pj}, the optical feedback strength κ_j, and the feedback delay times τ_j. The small signal gain is G_{0j}, the transparency population inversion is N_{0j}, and the gain saturation coefficient is ϵ_j. With the parallel coupled circuit configuration the total pump current is split among the lasers as $J_0 = J_1(t) + J_2(t)$. The variations of each current are assumed to depend linearly on the carrier population difference. Therefore

$$J_1(t) = J_0/2 - \eta[N_1(t) - N_2(t)] \tag{4}$$

and $J_2(t) = J_0 - J_1(t)$. The value of the coupling coefficient η is determined from our experimental data taken with a single laser having feedback. The threshold pump currents are given by $J_{\mathrm{th}j} = [N_{0j} + (\tau_{pj}\ G_{0j})^{-1}]\,/\tau_{sj}$. The two lasers are similar so that, in most calculations, we assumed the parameters summarized in Table I. They have been attributed values according to early studies [6,7,17] and had fine adjustments

TABLE I. Parameter values used in numerical simulations.

α_j	3.0	G_{0j}	1.2×10^4 s^{-1}
N_{01}	1.0×10^8	N_{02}	0.99×10^8
$1/\tau_{pj}$	513×10^9 s^{-1}	$1/\tau_{sj}$	0.5×10^9 s^{-1}
$\kappa_1 = \kappa_2$	16×10^9 s^{-1}	ϵ_i	5.0×10^{-7}
$\tau_1 = \tau_2$	40 ns	η	2.5×10^8 s^{-1}

by inspection of our experimental data. The pump current was taken as $J_0 = 2.03 J_{th1}$. The numerical solutions were obtained with a standard fourth order Runge-Kutta algorithm. With the parameters used, the fastest time scale was set by $\tau_p \sim 2$ ps and integration time steps were fixed at $dt = 0.2$ ps. Transients spanning 100 external cavity-feedback times were discarded in the solutions. The robustness of the results with respect to small parameter variations was verified. Comparisons between theory and experiment are presented next.

IV. EXPERIMENTAL AND THEORETICAL RESULTS

Let us now give the experimental results along with the theoretical numerical integration of our equations. Segments of the lasers power when only one laser has optical feedback are presented in Fig. 2(a). The signal corresponding to laser 1, operating with optical feedback, is given in the top lines (displaced for easier visualization). The chaotic nature of the dynamics in laser 1 appears in the irregular time interval between LFF drops. Laser 2 (lower line) was electrically coupled but did not have optical feedback. It presents jump up spikes in optical power, acting as a kind of sensor for the chaos in laser 1 via their electronic dynamics. Figure 2(b) shows equivalent segments of the calculated time series. The value of η for the equations was extracted from the experimental signal by matching the relative amplitude for the drop and jump up. It corresponds to a current partition deviation from $J_0/2$ of $\delta J_i \approx \pm 10^{-3} J_0$ at the spikes of LFFs and jump ups. Direct measurements of the current fluctuations are given in Sec. V.

A single laser, pumped by a constant current, has less carrier recombination in its junction region when its power output decreases. This means an increase of junction voltage, as observed by Ray *et al.* [21]. The number of junction carriers increases and the physical picture representing current voltage in a direct polarized ideal diode under feedback light gives a consistent explanation to these results. Here, with the parallel coupled lasers, the total current is constant but the current in each laser can vary. The consequence is observed in Fig. 2. Each time laser 1 has an optical power drop, there is a decrease of its current and the correlated increase in the current of laser 2 implies a jump up of its power (lower line). The ultrafast fluctuations (tens of picoseconds) are not observed in our experimental conditions. Our detection is not sensitive at the ultrahigh frequencies.

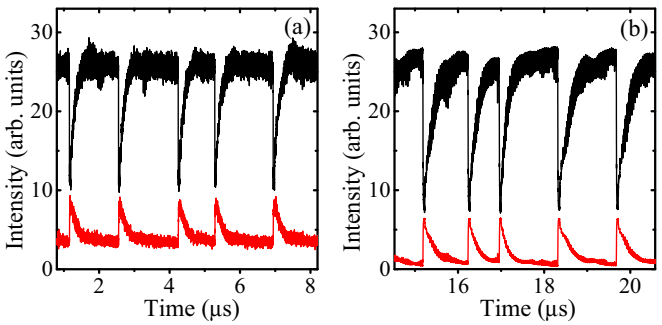

FIG. 2. Output power of the coupled lasers. Laser 1 (top line) that has optical feedback shows LFF power drops, while laser 2 (lower line) had no optical feedback. (a) Experimental light intensity and (b) $|E_j(t)|^2$ from numerical integration of Eqs. (1)–(3) (the vertical scales were displaced for better visualization).

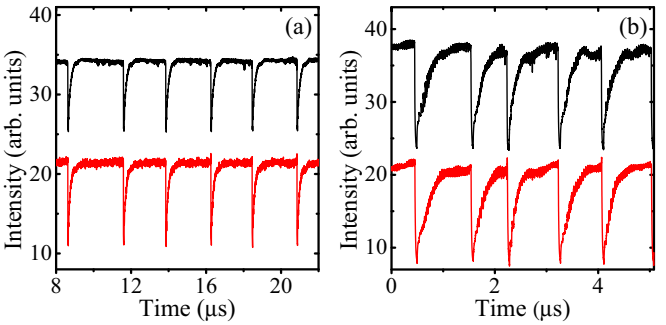

FIG. 3. Output power of the lasers coupled in parallel and having optical feedback. The top line is laser 1 and the bottom is laser 2. (Power scales were displaced for visualization.) Synchronism is clearly observed. (a) Experimental time series including a few power drops. (b) Numerical integration for the coupled laser equations.

Drops in light emission from one diode source accompanied by an emission increase from another one electrically connected in parallel were reported a long time ago for light-emitting diodes [1] and lasers [2]. These were experiments in fluctuations around stable operation conditions different from the emphasis of our work.

Chaotic dynamics in the parallel electronic coupling scheme shows more than simply antiphase correlations. Novel results are revealed when both lasers have optical feedback. In general, each laser can manifest uncorrelated LFF power drops. However, as seen in Fig. 3(a), when we choose appropriate experimental alignments and value for the total current, the large power drops synchronize in phase. Now, instead of an increase of one laser power, at the expense of the big drop in the other one, both lasers have nearly simultaneous LFF power drops. Figure 3(b) shows a comparable numerical segment of the lasers power calculated using the coupling parameter η obtained from the data with a single laser having the feedback, as in Fig. 2(a). The small antiphase fluctuations are always present in any of the dynamical conditions, independent of LFF synchronization.

These antiphase fluctuations at a time scale above nanosecond are clearly observed as we look into short segments of the time series as shown in Fig. 4. They were also measured

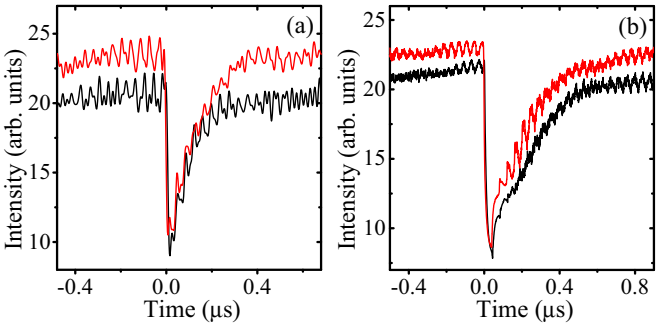

FIG. 4. Signal showing antiphase fine structure fluctuations superimposed on a pair of drops of the in-phase synchronized LFF when $\kappa_1 = \kappa_2$. (a) Experiment and (b) theory.

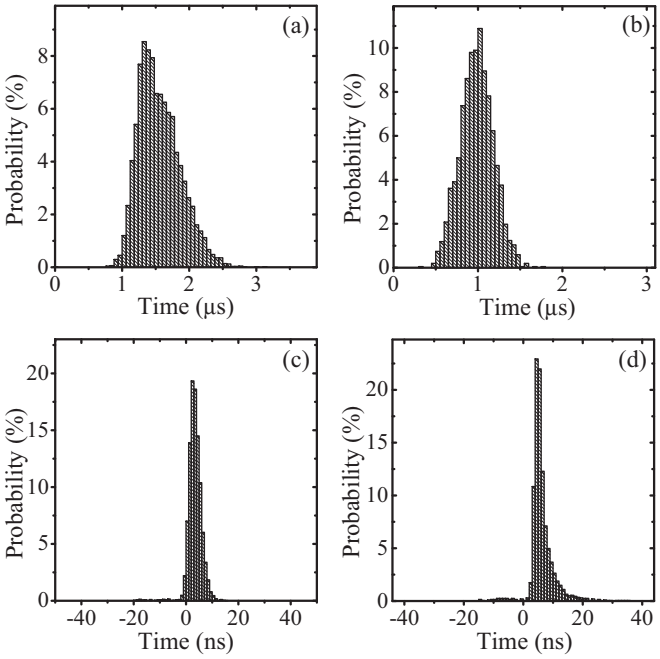

FIG. 5. Experimental LFF time interval histograms: (a) Time interval between successive drops in one of the lasers. (b) Theory for (a). (c) Time interval between drops of the two lasers. (d) Theory for (c).

directly in the voltages and currents variation on each laser (see Sec. V).

To better characterize the dynamics of the coupled system, histograms of events and correlation functions were made from experimental data series. Within full synchronism typical data series containing more than 10^5 events are captured without unpaired drops. The chaotic nature of the LFF drops shows in the broad histograms for the time interval between consecutive drops in any one of the lasers. These distributions, shown in Figs. 5(a) and 5(b), approximate Gaussians with an average time between drops of 1.5 μs, which is 37 times the feedback time, and a wide variance close to 1 μs. Both quantities are more than one order of magnitude larger than the lasers feedback time. The synchronization indicator is represented in the histograms given in Figs. 5(c) and 5(d). The time difference between the power drops of the two lasers has a very narrow distribution, with a width on the order of 10 ns, centered near zero delay. This is much narrower than the distributions shown in Figs. 5(a) and 5(b) for the time interval between successive pulses of a single laser, whose widths are on the order of 1 μs.

Notice in Fig. 5(c) that almost all pairs of drops occur within less than 10 ns, which is significantly shorter than the experimental 40 ns of optical feedback time. The small shift of a few nanoseconds from zero delay is sensitive to experimental unbalance of laser parameters. When one laser has a higher value for its feedback coefficient and/or a lower threshold and/or higher pump current in the parallel coupling circuit it becomes leading in the drops. The effects of small unbalances on the synchronism shifts were confirmed in the theoretical-numerical solutions as shown in Fig. 5(d). Bimodal distributions, with symmetrical anticipations and delays in the

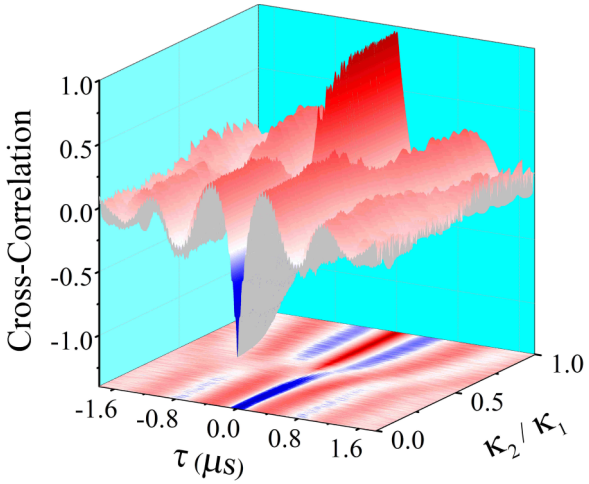

FIG. 6. Theoretical numerical cross-correlation dependence on the feedback coefficient ratio.

synchronizations, were also observed in experimental data and obtained in the theory, as we properly bias the parameters.

The onset of LFF synchronism depends on the feedback coefficient in each laser and on their coupling impedance. We present next how the synchronism transition, calculated as a function of the parameters κ_2/κ_1 and η, manifests in the cross-correlation functions $C(\tau)$ shown in Figs. 6–8. The calculation with the constant coupling parameter had η from Table I. Laser 2 is assumed to increase its feedback coefficient κ_2 from zero to $\kappa_2 = \kappa_1 = 16 \times 10^9$ s^{-1}. Figure 6 shows the calculated cross-correlation function. For zero and very small optical feedback in [aser 2, when no LFF exists in this laser, only antiphase fast oscillation and the jump ups are present, as in Fig. 2. This gives the value of -1 for the zero delay, $\tau = 0$, cross correlation. As κ_2 increases, LFF drops start to appear in laser 2 and some drops coincide with those in laser 1. Positive contributions begin to add to the cross correlation. At some intermediate value of κ_2, $C(\tau = 0)$ vanishes. This does not mean that the signals are totally uncorrelated. It does show that in-phase and antiphase fluctuations, in different time scales, are simultaneously present in the dynamics. The full chaos synchronized LFF dynamics only appears with $\kappa_2/\kappa_1 > 0.7$ and the cross correlation is almost $+1$ (there is an ever-present small antiphase contribution). Cross sections of the three-dimensional (3D) Fig. 6 can reveal the onset of LFF synchronization when we plot $C(\tau = 0)$ as a function of κ_2/κ_1. It can also show the antiphase fluctuations in the graph of $C(\tau)$ for $\kappa_2 = 0$. These are given in Figs. 7(a) and 7(b), respectively.

The cross-correlation function was also calculated varying the electronic coupling coefficient to show the onset of LFF synchronization, starting with the two lasers having independent LFFs. This is given in Fig. 8. Very small values of η are unable to mediate the synchronism. Therefore the two lasers have LFF drops but they are independent and their cross correlation is null. As the value of η increases, a transition region is reached where more and more LFF pairs drop near simultaneously. At the value of $\eta = 1.2 \times 10^8$ s^{-1} full synchronism is attained and $C(\tau = 0)$ rises to the value near $+1$. This value of η corresponds to a peak coupling current of 50 μA as shown in Sec. V.

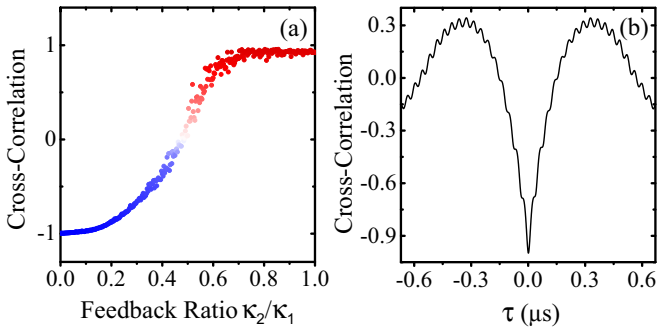

FIG. 7. Detail of Fig. 6. (a) Cross correlation between the lasers calculated at zero delay time ($\tau = 0$) as a function of κ_2/κ_1. (b) Cross correlation between the lasers calculated when laser 2 has no feedback ($\kappa_2 = 0$).

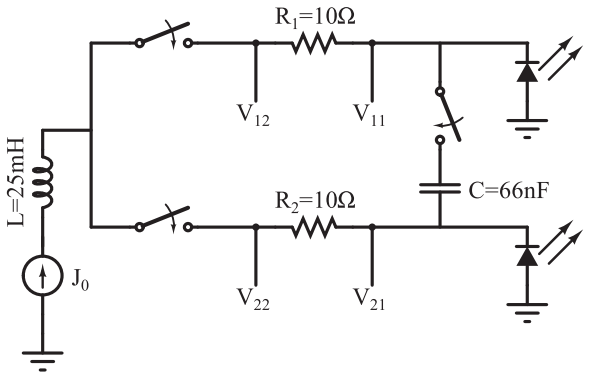

FIG. 9. Setup for the experiments on the power correlations and chaos synchronization of two electrically coupled lasers.

V. ELECTRICAL MEASUREMENTS IN THE COUPLED LASERS

We describe here details of the electrical measurements made along with the optical measurements on the coupled lasers. The lasers were coupled electrically in parallel configuration and pumped by a high impedance current source, as indicated in the electronic circuit shown in Fig. 9. The resistors R_1 and R_2 were included with two purposes. First, they controlled the amount of coupling between the lasers. Their values partially determine η, the current coupling coefficient, through the partition of the total current by Kirchhoff's laws $J_1(t) + J_2(t) = J_0$, supplemented by a linearized approximation for the currents unbalance as a function of the carriers populations,

$$J_1(t) = J_0/2 - \eta[N_1(t) - N_2(t)]. \quad (5)$$

$N_i(t)$ is the active carrier population of laser i with $i = 1,2$. The internal resistances of the lasers are smaller than 5Ω [2]. The value of η decreases with the circuit impedance between the lasers. Without the capacitor C such impedance is dominated by the external resistors. Consistently, we verified that when $R_1 = R_2 \geqslant 50\ \Omega$, the coupling is reduced to the point of preventing LFF synchronism. With these high values, optical power measurements with just one laser having optical feedback, like the one reported in Fig. 2, did not show a detectable response on the second laser without feedback. This evidences small coupling and explains why the two lasers with optical feedback had LFF but never got synchronized. The switch in Fig. 9 that shunted the capacitor C across the resistors could restore the synchronization, demonstrating that the precise value of η depends on more than circuit resistors. Our model provides remarkable agreement with the optical and electrical measurements, as described below. The second use of the resistors was to obtain the laser currents through the voltages V_{11}, V_{12}, V_{21}, and V_{22} on the extremes of the resistors. For that case we took small values $R_1 = R_2 = 10\ \Omega$ so that we had synchronism.

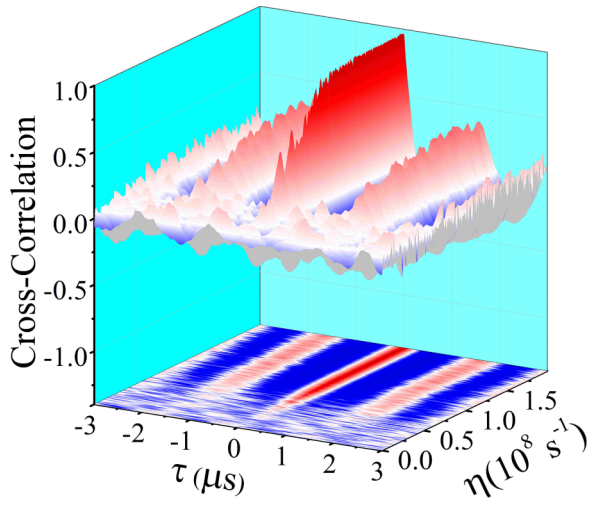

FIG. 8. Theoretical numerical cross-correlation dependence on the coupling coefficient η. Same parameters from Table I but $N_{02} = 0.998 \times 10^8$ and $J_0 = 2.02 J_{th1}$.

We made most of our measurements on the L780P010 and L850P010 Thorlabs lasers. Optical feedback was implemented by mirrors located at distances between 3.00 and 8.00 m from each laser. The feedback field coefficients κ_i were determined by the current threshold reduction, which could reach 6% in both lasers by proper alignment of the feedback mirrors. The pump current was near twice the (almost equal) single laser solitary threshold. Data series were acquired by fast (> 3 GHz band) photodiodes and a digital oscilloscope having a bandwidth of 1 GHz and a maximum sampling rate of 5 GS/s. The time series were computer treated to achieve averages and experimental histograms. The results for the measurements and numerical calculations with the dynamical equations are shown in Figs. 10–13.

Figures 10 and 11 correspond to the situation when only laser 1 has optical feedback and undergoes LFF pulsations, while laser 2 is affected by the current redistribution. Notice in Fig. 10(a) that there is a time mismatch of nearly 5 ns, which corresponds to 1/10 of the feedback time. Such time mismatch is attributed to electronic delays on the laser interconnections. It was accounted in the theoretical model by means of an unbalance in the lasers parameters. The corresponding measured pump currents obtained for the case of only one laser with feedback is given in Fig. 11. From these data we extract values between 30 and 130 μA for the spikes in the currents. These are fluctuations at least one order of magnitude larger than any thermal or quantum noise current fluctuation.

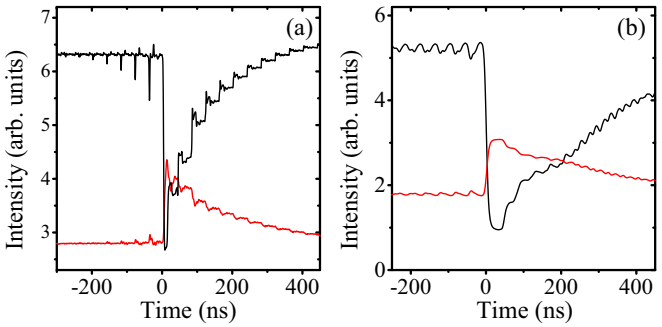

FIG. 10. Laser power variations during the LFF drop when only laser 1 had feedback. (a) Experimental. (b) Theory with $J_0/2 = 1.01 J_{\text{th}_1}$ and $J_{\text{th}_1} = 7.87\,503 \times 10^{16}\ \text{s}^{-1}$. In both figures the black curves correspond to laser 1 and the red (online) curves to laser 2.

The results for a pair of synchronized drops, when both lasers have optical feedback, is given in Figs. 12 and 13. Again there is the time mismatch of nearly 5 ns, which corresponds to 1/10 of the feedback time. They show clearly that the signals do not drop on exact time coincidence. However, on the coarse grained (many nanoseconds) time scale both laser powers always drop together. The comparison with the model here is excellent when we substitute $J_0 = 20$ mA, obtaining an excursion of current variation equivalent to the experimental value of $\pm 30\ \mu$A, as shown in Fig. 13.

VI. THE ONSET OF SYNCHRONISM

When the two lasers have optical feedback each one can manifest LFF power drops which, in general, are uncorrelated. Still the small antiphase fluctuations are present. The onset of LFF synchronizations in time series is shown in Fig. 14(a). The two lasers have LLF but only a partial number of LFF drops in synchronism is observed. In these cases, instead of an increase of one laser power at the expense of the big drop in the other one, both lasers drop power together. Figure 14(b) shows a numerical time series giving a segment calculated with the parameter η varying in this intermediate synchronism regime.

The rate equation model reproduces this dynamical condition as shown in Fig. 14(b). As we choose an appropriate value for the total current and feedback alignments, more and

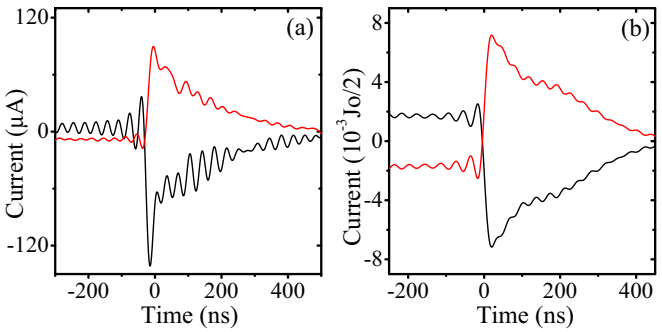

FIG. 11. Pump current variations during one LFF drop of laser 1 while laser 2 had no feedback. (a) Experimental. (b) Theory. In both figures a 29 MHz low-pass filter was used. The black curves correspond to laser 1 and the red (online) curves to laser 2.

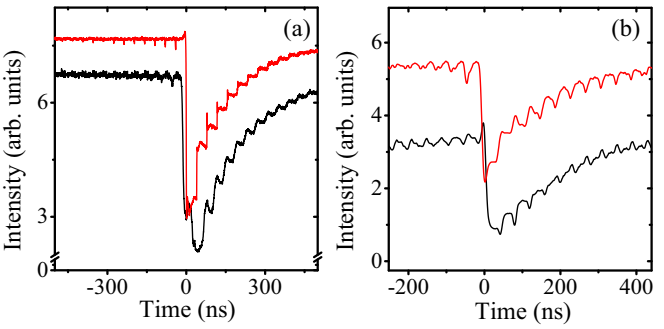

FIG. 12. Laser power variations during a pair of synchronized LFF drops. (a) Experimental. (b) Theory with $J_0/2 = 1.01 J_{\text{th}_1}$ and $J_{\text{th}_1} = 7.87\,503 \times 10^{16}\ \text{s}^{-1}$. In both figures the black curve corresponds to laser 1 and the red (online) curve to laser 2.

more cases occur where both lasers have a near simultaneous irregular LFF power drop until all power drops synchronize in phase with a small time mismatch of a fraction of the feedback time. Both the experimental and the numerical theoretical curves showing intensity drops and current jumps during a synchronized LFF reveal a delay time between the two lasers. In the experimental system this delay was traced to the threshold of the lasers. The one with a lower threshold, on the order of 2%, always dropped a few nanoseconds earlier. Consistently, introducing a 1% difference among the numerical values of threshold in the equations did reproduce the same type of delay. A quantitative inspection of LFF delay versus the other parameters was left for further studies. Also, investigation of the role of significant electronic delays, by changing the length of the circuits wiring, will be left for a future work. In our current experiments, cables of less than 10 cm restricted the possible delay to less than a nanosecond. Therefore, our observed delays, associated to threshold parameters, have a physical origin on the carriers electronics in the junctions.

VII. ON THE PHASE OF THE CHAOTIC INTENSITY PULSES AND THE OPTICAL PHASE OF THE FIELDS

The concept of synchronized chaotic optical oscillators described here deserves clear distinction from the concept of

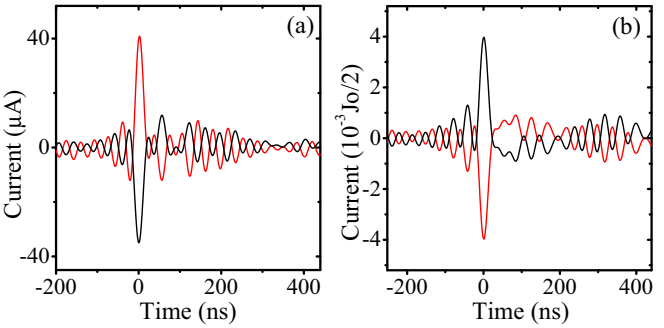

FIG. 13. Pump current variations during a pair of synchronized LFF drops. (a) Experimental. (b) Theory with $J_0/2 = 1.01 J_{\text{th}_1}$ and $J_{\text{th}_1} = 7.87\,503 \times 10^{16}\ \text{s}^{-1}$. In both figures a 29 MHz low-pass filter was used. The black curves correspond to laser 1 and the red (online) curves to laser 2.

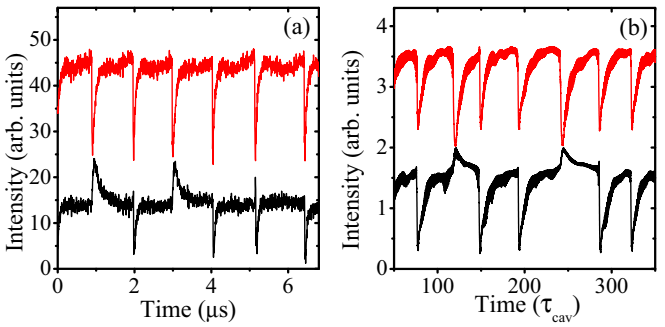

FIG. 14. Output power of the lasers coupled in parallel and having optical feedback. The pump current and feedback strengths were set to partial synchronism of LFF. The top line is laser 2 and the bottom is laser 1. (Power scales were displaced for visualization). (a) Experimental and (b) numerical integration from theory. Whenever a coincidence drop is missed there is a power jump up in one of the lasers.

synchronization by frequency entrainment in optical clocks. This last case demands that the two optical fields evolve in time with a locked phase as

$$E_j(t) = |E_{0j}(t)| \exp[-i\phi_j(t)], \tag{6}$$

with $\phi_1(t) - \phi_2(t) = \text{const}$.

Most of the chaos synchronization among lasers does not obey such condition. This is the case here. Both in the experimental and numerical cases, we focus on the light intensity dynamics obtained from the squared field amplitude. The irregular pulses described by $I_1(t)$ and $I_2(t)$ are the result of a time averaging over optical periods and even more, averaging over detection time filtering. Therefore, we are dealing with phases on intensity variations rather than amplitude oscillations. The phases that we get for the dynamical variables in their phase spaces can appear as locked when chaos synchronization is attributed to the coupled dynamics but there is no locking of the optical phase. Specifically, the averaged winding numbers calculated for the two slowly varying field envelopes in our rate equations became equal in the condition we call synchronous. Detailed discussions on the phase synchronization in coupled chaotic oscillators can be found in [22,23].

We can investigate the behavior of the optical phases from the numerical time series for the complex field amplitudes. Figures 15(a)–15(f) show the optical phases and frequencies calculated from Eqs. (1)–(3) when the lasers have synchronized LFF. It is important to notice that in Fig. 15(b) the phases evolve with respect to the solitary laser phases, given by $\omega_0 t$, while most of the time the lasers have a redshifted frequency near the maximum gain condition. From the calculated slope we infer that circa 300 external cavity modes, separated by $\Delta\omega = 25$ MHz, participate in their itinerant dynamics [7]. The difference among the two phases is near zero in a rough coarse grained time scale as seen in Fig. 15(c). The numerical time derivative of the phases give the instantaneous frequency. The value for each laser is shown in Fig. 15(d) where they appear superimposed.

During each pair of drops, which appear to be simultaneous when viewed in a large time scale (tens of nanoseconds), the

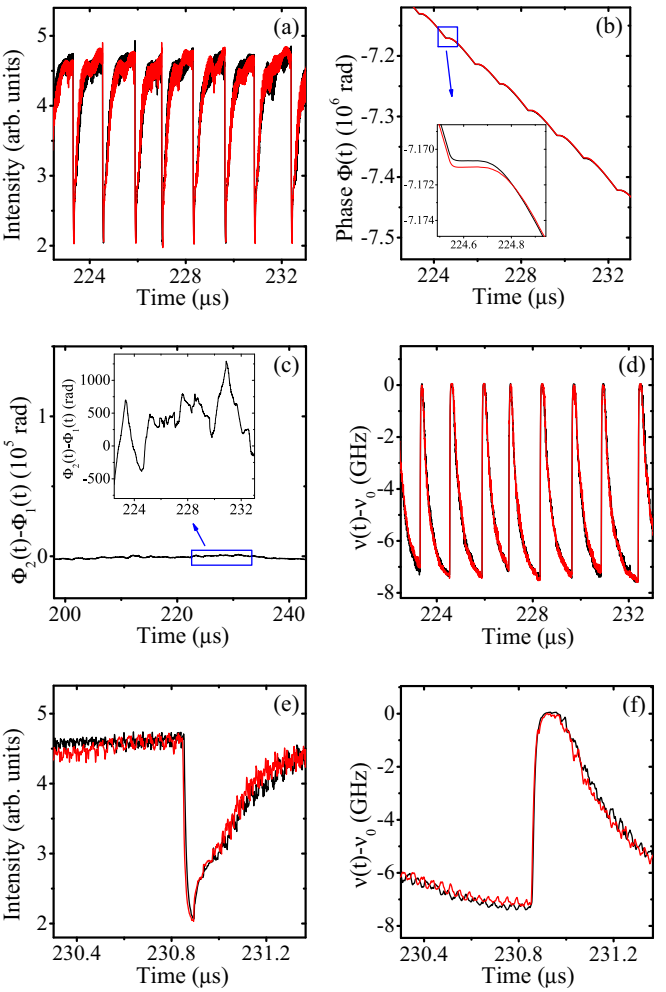

FIG. 15. Numerically calculated optical phase for the two coupled lasers. (a) Segment of the laser intensity for the sake of comparison. (b) Plot of the two phases evolving in time. (c) Phase difference showing the large time scale synchronism. (d) Optical frequency excursion of the two lasers. (e) Details of the intensity fluctuations close to a synchronized drop and (f) the instantaneous frequency of the two lasers.

two lasers can have different optical phases with jumping excursions of thousands of radians. In Fig. 15(c), the phase mismatch is shown in two short time intervals around LFF drops. Notice that the short time (tens of nanoseconds) oscillations of the phases are partially synchronized in antiphase. The single drops, with a shorter time scale permits the observation of the anticorrelated fast oscillations both in the intensities and in the optical phase at different time intervals before the drop. The (7.5 GHz) irregular red frequency chirping during each LFF drop and recovery cycle is clearly observed in Fig. 15(f). In all cases a precise optical synchronism is never attained, consistent with our experiments.

VIII. ON THE CORRELATION FUNCTIONS

The proper setting for synchronization could give long data series containing more than 10^5 LFF events missing no pair of simultaneous drops. The competition for pump energy still

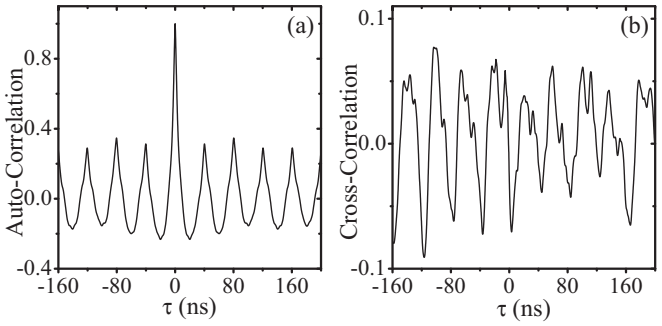

FIG. 16. Experimental correlations of the lasers coupled in parallel and having optical feedback. (a) Autocorrelations of one laser. (b) Cross correlation showing negative values due to antiphase fluctuation contributions, superimposed to large time scale positive contributions due to in-phase fluctuations.

exists, but only in short time scale intervals. Figure 16(a) shows the autocorrelation function calculated from experimental series measured for one laser to compare with the experimental cross correlation between the two synchronized lasers in Fig. 16(b). The theoretical autocorrelation function for one laser and cross correlation for the two synchronized lasers are shown in Fig. 17.

Autocorrelation and cross-correlation functions of signals having more than one dominant (not necessarily perfectly periodic) period need interpretation when one wants to identify in-phase, positive correlated, and antiphase, negative correlated signals. To clarify how in-phase synchronized signal

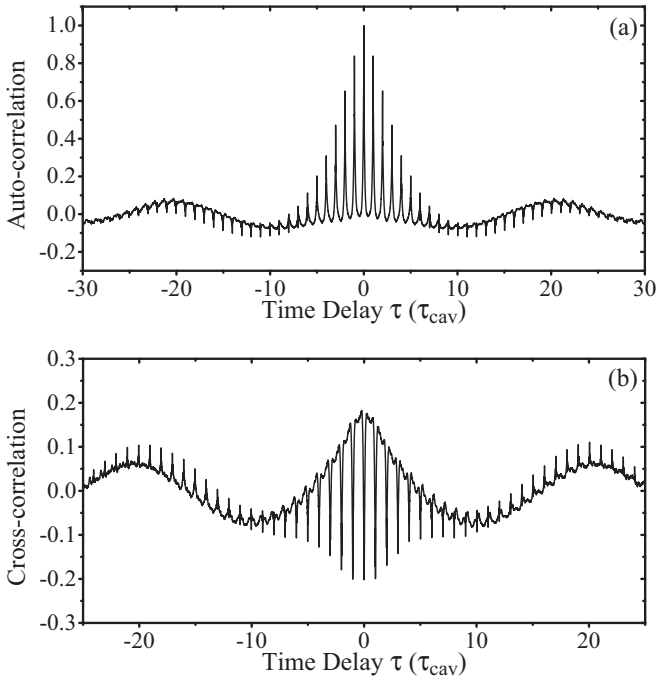

FIG. 17. Numerical correlation functions: (a) Autocorrelation of laser 1. (b) Cross correlation showing the downgoing antiphase fine structure superimposed on the in-phase synchronized LFF. Filters were used to enhance the proportions of antiphase (negative contribution) and in-phase (positive contribution) signals visible.

events in slow time scale coexisting with some antiphase oscillations of individual units in a coupled system manifest in cross-correlation functions, we did numeric calculations using nonchaotic time series extracted from the functions

$$X(t) = A\ \cos(\Omega_1 t) + a\ \sin(\omega_1 t),$$
$$Y(t) = B\ \cos(\Omega_2 t) + b\ \sin(\omega_2 t). \tag{7}$$

When Ω_1/Ω_2 and ω_1/ω_2 are not rational, the cross correlation between these signals is zero. Interesting results appear when we consider $\Omega_1 = \Omega_2 = \Omega$ and $\omega_1 = \omega_2 = \omega$ and change the values of the coefficients. The cross correlations of these signals will give clues to what we get for the cross correlations from the nonlinear equation for the electrically coupled lasers having optical feedback.

Taking a total time much larger than $1/\Omega$ and $1/\omega$, the analytical expressions for the autocorrelation C_1 and cross correlation C_{12} at $\tau = 0$ between the signals become

$$C_{12}(\tau = 0) = \frac{\langle \Delta X \Delta Y \rangle}{\sqrt{\langle (\Delta X)^2 \rangle \langle (\Delta Y)^2 \rangle}} = \frac{(AB + ab)}{\sqrt{(A^2 + a^2)(B^2 + b^2)}}. \tag{8}$$

Our interest is when ω is at least one order of magnitude larger than Ω and the two time scales have opposite correlations. This is the case when $AB > 0$ and $ab < 0$, for example. Let us take A fixed and positive, and increase the value of B starting from zero. If $A \gg a$ and $B \gg b$ we have $C_{12} \to +1$ and, conversely, if $A \ll a$ and $B \ll b$ we have $C_{12} \to -1$. To visualize the numerically calculated figures, we took $A = 105$, $a = -b = 33$, $\Omega = 2\pi$, and $\omega = 20 \times 2\pi$. Varying B from zero to the value of A we get the calculated cross correlations shown in Figs. 18 and 19. For small B the antiphase contribution from the two fast sinusoidal signals dominates. This is seen in the negative portion of the cross correlation at a zero time.

The cross correlation of the laser dynamics in chaos have qualitatively the same shape seen in the respective figures above. We can therefore interpret the onset of LFF synchronism obtained in our experiments by inspection of these correlation functions.

IX. RELATED DYNAMICS IN MULTIMODE LASERS

The dynamics of coupled monomode laser oscillators have general features common to the dynamics of single lasers with more than one field mode. Such common properties result from the fact that the number of dynamical variables in both systems can be the same. Two monomode lasers, like the ones described by our equations, before optical feedback is included, consist of a pair of three-dimensional dynamical systems: one complex field, $E_i(t)$, and one gain population, $N_i(t)$, for each. A single laser like a vertical-cavity surface-emitting laser (VCSEL), when described as two polarization modes [24–26], also has two orthogonal fields, $E_+(t)$ and $E_-(t)$, competing for two populations, $N_+(t)$ and $N_-(t)$. These are associated to the different subbands as proposed by San Miguel *et al.* [24]. The interlasers coupling mechanism in our case is attributed to Kirchhoff's law as current conservation in the parallel circuit,

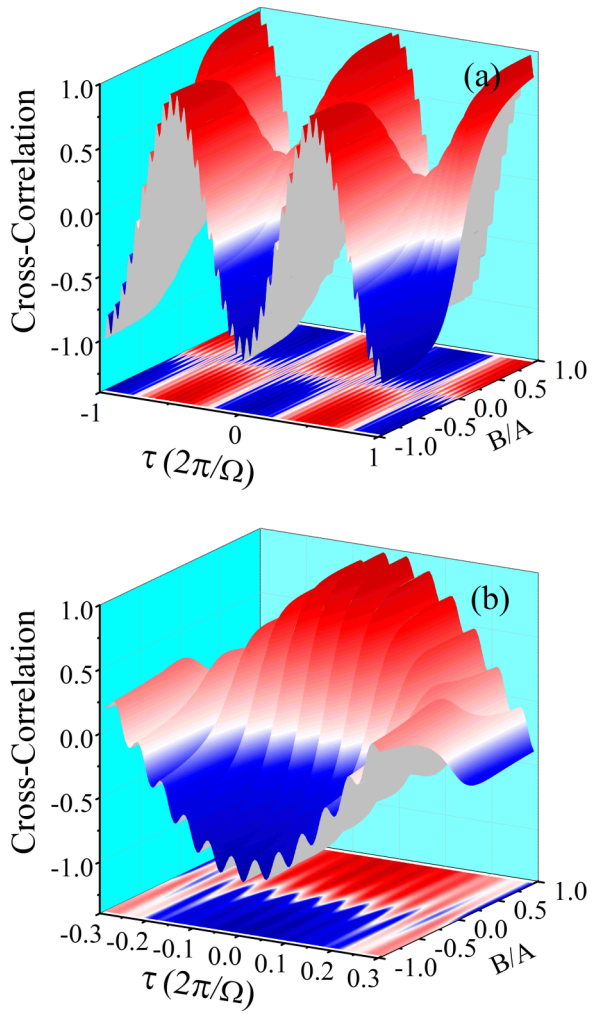

FIG. 18. Numerical cross correlation obtained when two simple signals are composed by harmonics in phase and antiphase, with different frequencies and having variable amplitudes. (a) 3D map showing the dominant antiphase term contribution evolving to the in-phase cross correlation when B in Eq. (7) varies from $-A$ to A. (b) Details of (a) showing the undulations associated to antiphase overriding the wide positive correlation curves.

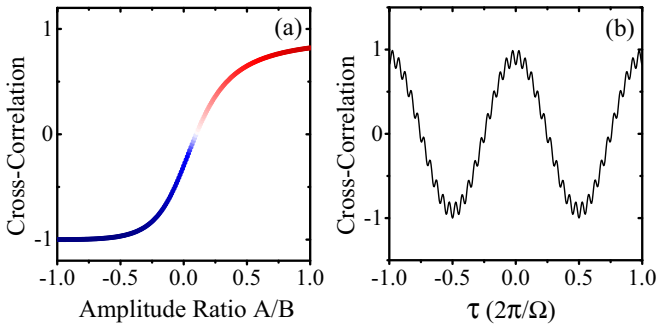

FIG. 19. Details of the numerical cross correlation obtained when two simple signals are composed by harmonics in phase and antiphase with different frequencies and having variable amplitudes. (a) Variation of the zero time ($\tau = 0$) cross correlation showing the excursion from fully antiphase, -1, to almost complete in phase near $+1$. The value $+1$ is not reached because a small antiphase contribution is always present. (b) Correlation profile when $B = A$.

while the two populations in the VCSEL model are coupled by spin-flip mechanisms. The introduction of optical feedback in either system brings the infinite dimensional feature depending on time delay and the two subsystems show LFF [25]. Antiphase and in-phase correlations among the two laser intensities $I_1(t)$ and $I_2(t)$, as for I_+ and $I_-(t)$ in VCSELs, should therefore not be a surprise to be found in both systems. Also, intensity correlations between different spatial modes, both in edge emitting diode lasers and VCSELs, have been investigated long ago in Refs. [27–31], where the spatial distribution of intensity noise was measured and intermode anticorrelations were responsible for total intensity noise reduction, sometimes below the shot noise level.

The phase correlations in VCSELs are very well detailed in the paper by Sciamanna *et al.* [26]. These authors call attention to the need for more experimental work on the VCSEL dynamics and we hope to include such studies in our future research with coupled systems. A detailed description of the optical feedback effects in vertical-cavity surface-emitting and edge emitting semiconductor lasers is given by Panajotov *et al.* [32]. Edge emitting are the types used and described in our experiments, but we have evidence for the same effects with vertical-cavity surface emitting lasers. Discussions referring to the coexistence between fast antiphase oscillations within multimode LFF dynamics can be found in the literature [33,34].

X. CONCLUSION

We have thus demonstrated in detail how in-phase synchronized dynamical events in slow time scale can coexist with antiphase oscillations between individual units in a pair of coupled lasers. A remarkable observation, both in the experiments and in the simple theoretical model, is some enhancement of the antiphase oscillations amplitude just before any sharply synchronized power drop, as shown in Figs. 4(a) and 4(b) for the intensity, as well as in Figs. 13(a) and 13(b) for the current dynamics. We also obtained numerical cases where the antiphase enhancement before the drops appear on the frequency correlation. The variation of correlation signals with time scale shown here for two lasers is relevant to the study of multilaser networks and their use for simulation of complex systems. Pairwise correlations within a complex network are known to be distinct from correlations among large groups of units [35,36], as well as different from the correlations in a single coupled pair system [1]. Detailed knowledge of the properties of pair units will enlarge the possibility to extract properties resulting from the multicoupling topology in networks with many complex subsystems.

ACKNOWLEDGMENTS

This work is partially supported by Brazilian Agencies: Conselho Nacional de Desenvolvimento Científico e Tecnológico (CNPq), Coordenação de Aperfeiçoamento de Pessoal de Nível Superior (CAPES), Fundação de Amparo à Pesquisa do Estado do Rio de Janeiro (FAPERJ), and Fundação de Ciência de Pernambuco (FACEPE).

[1] P. J. Edwards and G. H. Pollard, Phys. Rev. Lett. **69**, 1757 (1992).

[2] P. M. Mayer, F. Rana, and R. J. Ram, Appl. Phys. Lett. **82**, 689 (2003).

[3] A. Z. Khoury, Phys. Rev. A **60**, 1610 (1999).

[4] C.-H. Lin, S.-P. Li, and K. Y. Szeto, *Artificial Economics and Self Organization*, Lecture Notes in Economics and Mathematical Systems Vol. 669 (Springer, New York, 2014), p. 71.

[5] Ch. Risch and C. Voumard, J. Appl. Phys. **48**, 2083 (1977).

[6] R. Lang and K. Kobayashi, IEEE J. Quant. Electron. **16**, 347 (1980).

[7] T. Sano, Phys. Rev. A **50**, 2719 (1994).

[8] A. Karsaklian Dal Bosco, D. Wolfersberger, and M. Sciamanna, Europhys. Lett. **101**, 24001 (2013).

[9] É. Mercier, A. Even, E. Mirisola, D. Wolfersberger, and M. Sciamanna, Phys. Rev. E **91**, 042914 (2015).

[10] M. Sciamanna and K. A. Shore, Nat. Photonics **9**, 151 (2015).

[11] M. Giudici, C. Green, G. Giacomelli, U. Nespolo, and J. R. Tredicce, Phys. Rev. E **55**, 6414 (1997).

[12] Manuel C. Eguia and G. B. Mindlin, Phys. Rev. E **60**, 1551 (1999).

[13] J. F. Martinez Avila, H. L. D. de S. Cavalcante, and J. R. Rios Leite, Phys. Rev. Lett. **100**, 044101 (2008).

[14] F. Selmi, R. Braive, G. Beaudoin, I. Sagnes, R. Kuszelewicz, and S. Barbay, Phys. Rev. Lett. **112**, 183902 (2014).

[15] M. C. Soriano, J. García-Ojalvo, C. R. Mirasso, and I. Fischer, Rev. Mod. Phys. **85**, 421 (2013).

[16] M. Nixon, E. Ronen, A. A. Friesem, and N. Davidson, Phys. Rev. Lett. **110**, 184102 (2013).

[17] G. H. M. Van Tartwijk and D. Lenstra, Quantum Semiclassical Opt. **7**, 87 (1995).

[18] V. Ahlers, U. Parlitz, and W. Lauterborn, Phys. Rev. E **58**, 7208 (1998).

[19] L. Wu, S. Zhu, and J. Li, Physica D **223**, 208 (2006).

[20] A. Argyris, D. Syvridis, L. Larger, V. Annovazzi-Lodi, P. Colet, I. Fischer, J. Garcia-Ojalvo, C. R. Mirasso, L. Pesquera, and K. A. Shore, Nature (London) **438**, 343 (2005).

[21] W. Ray, W-S. Lam, P. N. Guzdar, and R. Roy, Phys. Rev. E. **73**, 026219 (2006).

[22] A. S. Pikovsky, M. G. Rosenblum, G. V. Osipov, and J. Kurths, Physica D **104**, 219 (1997).

[23] M. G. Rosenblum, A. S. Pikovsky, and J. Kurths, Phys. Rev. Lett. **78**, 4193 (1997).

[24] M. San Miguel, Q. Feng, and J. V. Moloney, Phys. Rev. A **52**, 1728 (1995).

[25] M. Giudici, S. Balle, T. Ackemann, S. Barland, and J. R. Tredicce, J. Opt. Soc. Am. B **16**, 2114 (1999).

[26] M. Sciamanna, C. Masoller, F. Rogister, P. Mégret, N. B. Abraham, and M. Blondel, Phys. Rev. A **68**, 015805 (2003).

[27] A. Bramati, J. P. Hermier, A. Z. Khoury, E. Giacobino, P. Schnitzer, R. Michalzik, K. J. Ebeling, J. P. Poizat, and Ph. Grangier, Opt. Lett. **24**, 893 (1999).

[28] J. P. Hermier, A. Bramati, A. Z. Khoury, E. Giacobino, J. P. Poizat, T. J. Chang, and Ph. Grangier, J. Opt. Soc. Am. B **16**, 2140 (1999).

[29] J. P. Hermier, I. Maurin, E. Giacobino, P. Schnitzer, R. Michalzik, K. J. Ebeling, A. Bramati, and A. Z. Khoury, New J. Phys. **2**, 26 (2000).

[30] J. P. Hermier, A. Bramati, A. Z. Khoury, V. Josse, E. Giacobino, P. Schnitzer, R. Michalzik, and K. J. Ebeling, IEEE J. Quantum Electron. **37**, 87 (2001).

[31] C. L. Garrido-Alzar, S. M. de Paula, M. Martinelli, R. J. Horowicz, A. Z. Khoury, and G. A. Barbosa, J. Opt. Soc. Am. B **18**, 1189 (2001).

[32] K. Panajotov, M. Sciamanna, M. Arizaleta Arteaga, and Hugo Thienpont, IEEE J. Sel. Top. Quantum Electron. **19**, 1700312 (2013).

[33] G. Huyet, J. K. White, A. J. Kent, S. P. Hegarty, J. V. Moloney, and J. G. McInerney, Phys. Rev. A **60**, 1534 (1999).

[34] D. W. Sukow, T. Heil, I. Fischer, A. Gavrielides, A. Hohl-AbiChedid, and W. Elsäßer, Phys. Rev. A **60**, 667 (1999).

[35] E. Schneidman, M. J. Berry II, R. Segev, and W. Bialek, Nature (London) **440**, 1007 (2006).

[36] V. Pernice, B. Staude, S. Cardanobile, and S. Rotter, PLoS Comput. Biol. **7**, 1002059 (2011).